Electronic Supplementary Material (ESI) for Journal of Materials Chemistry A.

Supporting Information

Exceptional interfacial solar evaporation via heteromorphic PTFE/CNT hollow fiber array

Tiantian Li, Qile Fang, Jianqiang Wang, Haibo Lin, Qiu Han, Peng Wang and Fu Liu*

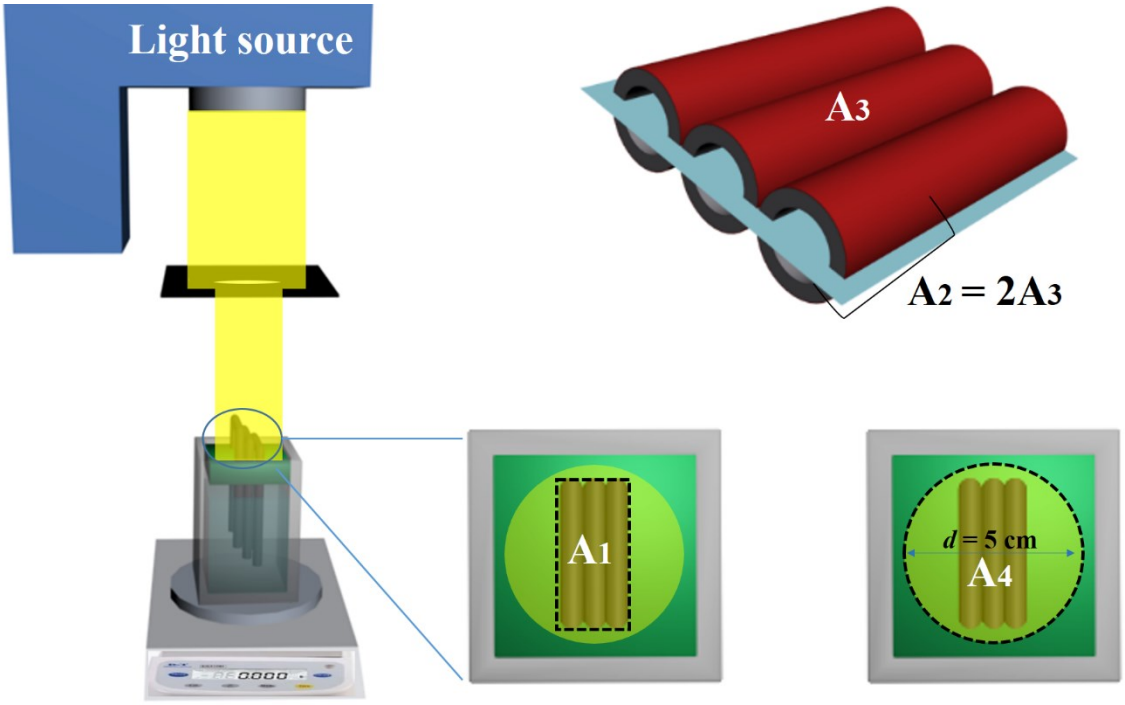

Supporting Scheme 1. The relationship of the projected area (A_1), evaporative area (A_2), illuminated area (A_3) and aperture area (A_4) for the heteromorphic evaporator.

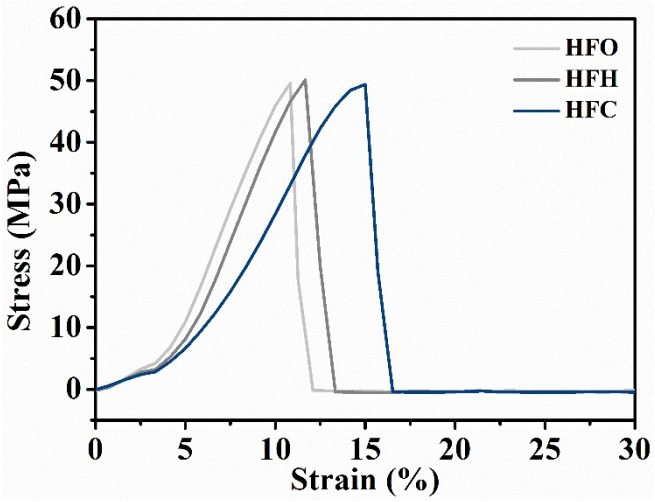

Figure S1. Mechanical properties for HFO, HFH and HFC, respectively. The tensile strain is extended from 10.8% to 15.0% after PDA/CNT modification due to the bio-adhesion effect.

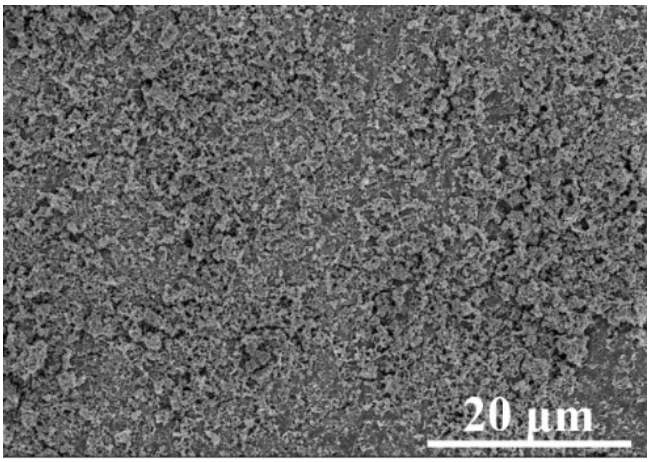

Figure S2. Outer surface morphology of HFC. It can be seen that the PDA and CNT were uniformly distributed on the surface.

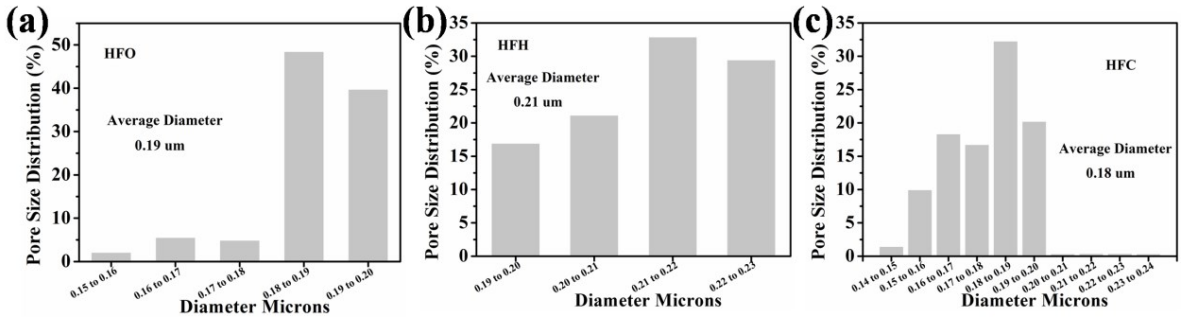

Figure S3. Pore size distribution for HFO, HFH and HFC, respectively. The mean pore size was 0.21, 0.19 and 0.18 μm, respectively.

The porosity was measured by comparing the weight of wet and dry membrane. The weight of membrane under dry state was measured and named as m_0. Then, the dry membrane was immersed into distilled water for 60 min until it was saturated with water. Lastly, the wet membrane was weighted (m_1) after whipping off excess surface water with filter paper and shaking off the water in the pipe. The porosity was determined according to Equation (S1).

$$Porosity(\%) = (m_1 - m_0) \times 100\% / \rho_{H_2O} V \qquad \text{(S1)}$$

where V is the volume of membrane under dry state and ρ is the density of water. The water holding capacity was also measured in the same way and calculated according to Equation (S2) and all the measured results were shown in **Figure S4** and **Table S1**.

$$Capacity(\%) = (m_1 - m_0) \times 100\% / m_0 \qquad \text{(S2)}$$

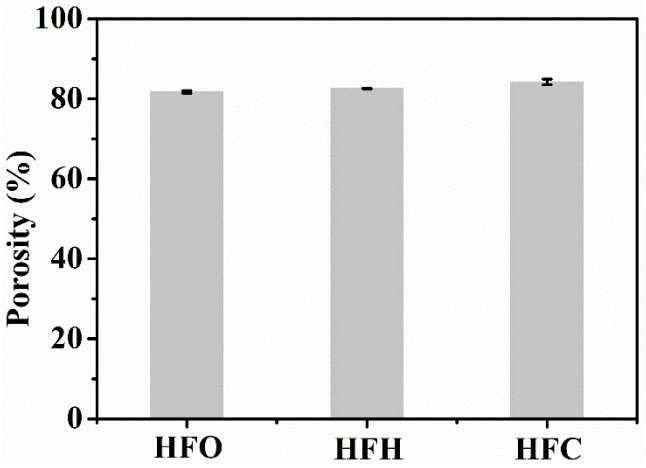

Figure S4. The porosity of HFO, HFH and HFC. The modified fiber keeps a high porosity of ~82%.

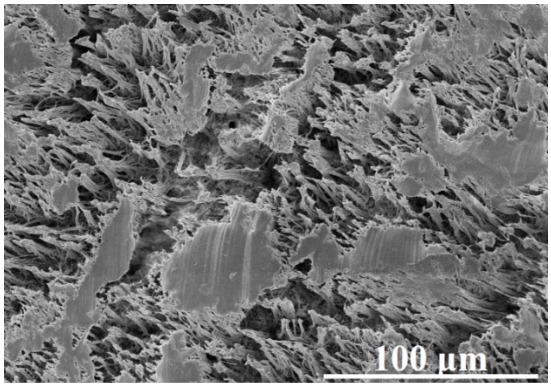

Figure S5. Magnified cross-section morphology of HFC. The periodical nano-fibrils are highly oriented parallel to the stretching direction.

Table S1. The water holding capacity for HFO, HFH and HFC, respectively.

Sample	Dry state (g)	Wet state (g)	Water (g)	Capacity (wt.%)	Average capacity (wt. %)
HFO	0.0691	0.0702	0.0011	1.6	2.1
	0.0691	0.0706	0.0015	2.2	
	0.0692	0.0710	0.0018	2.6	
HFH	0.0691	0.1728	0.1037	150.1	149.9
	0.0693	0.1730	0.1037	149.6	
	0.0693	0.1732	0.1039	149.9	
HFC	0.0650	0.1710	0.1060	163.1	162.7
	0.0660	0.1708	0.1048	158.8	
	0.0641	0.1706	0.1065	166.1	

The length of water on surface and in pipe for HFC was also measured. In detail, the membranes were vertically immersed into water at the same time with the depth of 2 cm. After equilibrium, the membranes were quickly removed from water to measure the weight, and then the water existence in pipe was blown out using an ear ball to measure the weight again. The water length was calculated according to the change of weight. It found that the height of water in pipe was not consistent with that on surface for sample HFH and HFC as listed in **Table S2** and **Figure S6**. More interestingly, the rising height of dyes in pipes is almost the same as that of water in pipes. The reason may be that the capillary force between fibers is stronger than that in pipe and most dyes can only rise with the water in the pipe, but not with the water between the fibers. For HFO, due to its hydrophobicity, it can't be wetted and dyed by aqueous solution of Congo Red.

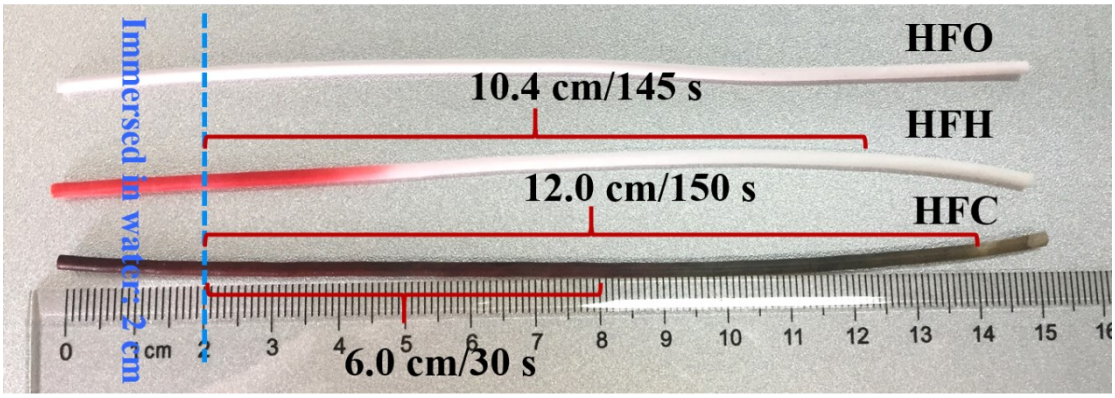

Figure S6. The water supply ability of HFO, HFH and HFC, respectively.

Table S2. The length of water existence on surface and in pipe respectively.

Sample	Total length (cm)	Surface Water length (cm)	Water length in pipe (cm)
HFO	15	0	0
HFH	15	10.4	1.91
HFC	15	12.0	1.78

*The length for immersed into water (2 cm) was subtracted from them.

The static BSA adsorption experiment was measured by BSA content change. The membranes with 5 cm length were immersed into 30 mL BSA solution of 1 g L^{-1} in PBS buffer solution at 25 ^{o}C. The hollow fiber membranes were maintained for 48 h until adsorption equilibrium. The change of BSA concentration was measured by UV–VIS-NIR spectrometer (Lambda 950, Perkin Elmer, US) at 280 nm. The change of BSA content in the solution is approximately equal to the amount of BSA adsorbed on the membrane surface and the amount of adsorption is calculated using the following Equation (S3).

$$P = (1 - C_t / C_0) \times V / S \times 1000 \qquad \text{(S3)}$$

where P (μg cm^{-2}) is the amount of BSA adsorbed on the membrane surface, C_0 and C_t (g L^{-1}) represent the concentration of BSA in solution at the initial moment and after adsorption equilibrium, respectively, V (30 mL) is the volume of the BSA solution, S is the area of the membrane including inner surface and outer surface.

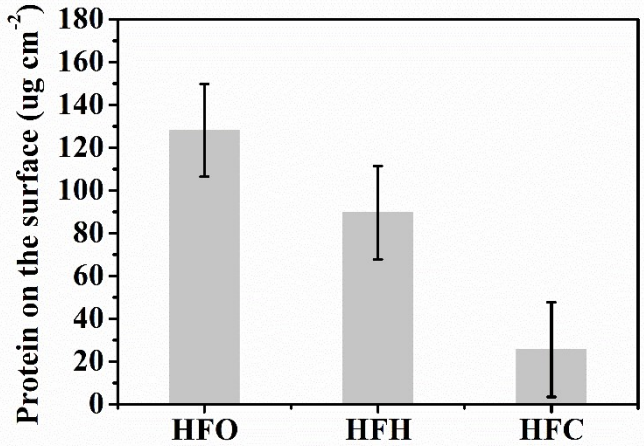

Figure S7. BSA static adsorption content on the surface of HFO, HFH and HFC.

It is noted that surface morphology and light performance can be seriously affected by the modification methods as exhibited in **Figure S8** and **Figure S9**. If only PDA was loaded, the light absorption properties would be compromised with only 85 %. In contrast, only 82% light can be absorbed if PDA and CNT were directly loaded on the surface of hollow fiber membrane without pre-loading PDA as the bio-glue layer. This indicated that the pre-loading of PDA as a mediation layer was important for the subsequent CNT loading.

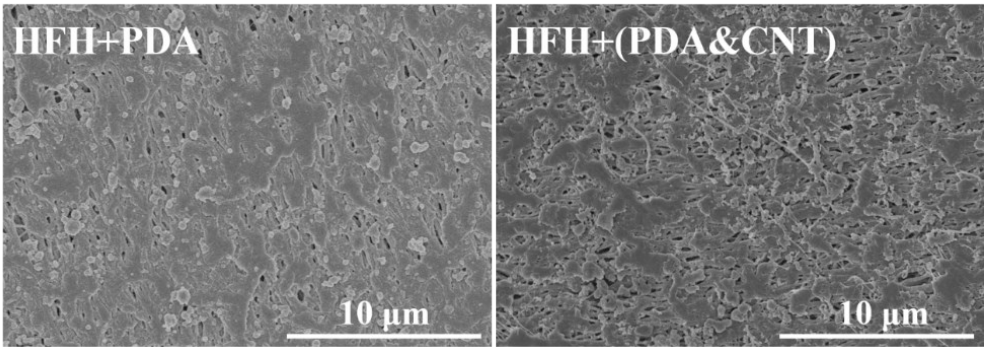

Figure S8. The morphology of PTFE hollow fiber membrane after solely loading PDA (left image) and directly loading PDA and CNT without pretreating (right image).

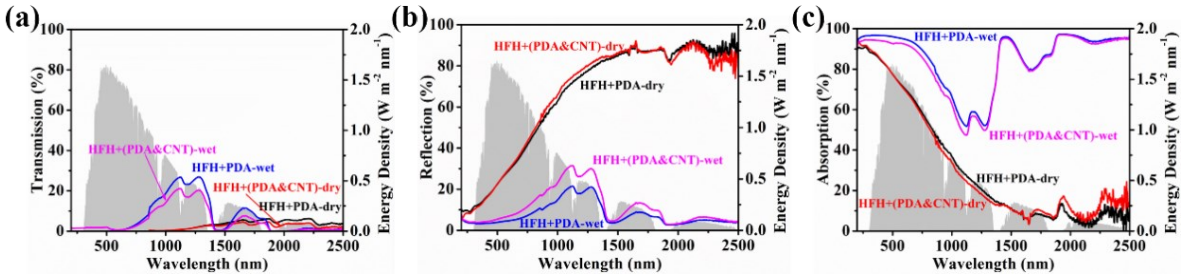

Figure S9. (a) Transmission, (b) reflection and (c) absorption performances of HFH+PDA and HFH+(PDA&CNT).

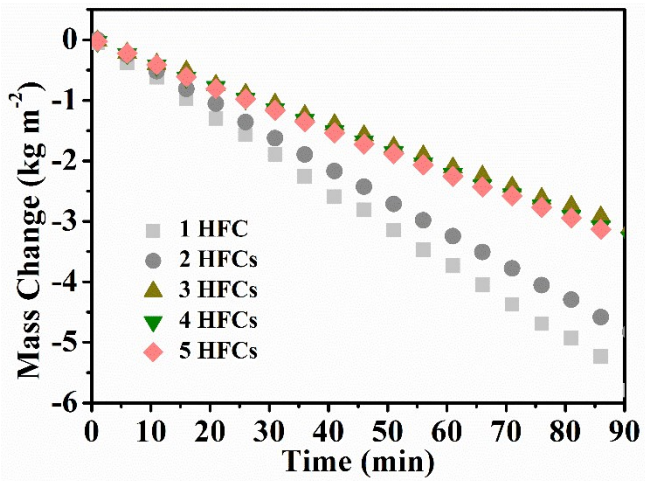

Figure S10. Time course of water evaporation performances for membrane arrays with multiple fibers aligned compactly (1, 2, 3, 4, 5), the evaporation rate declines from a high value of 3.73 kg m^{-2} h^{-1} to a nearly stable value of ~2.10 kg m^{-2} h^{-1} under one sun illumination.

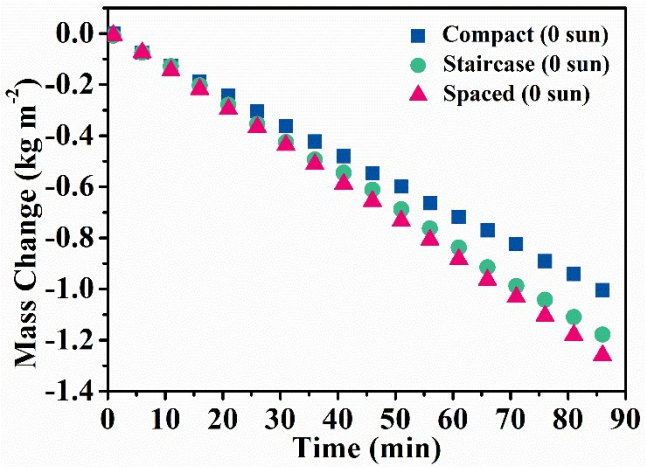

Figure S11. Mass changes with time for 3 HFCs arrayed with different style without illumination: compact, staircase and spaced manner. Base materials had little effect on natural evaporation under dark environment as shown in Table S3.

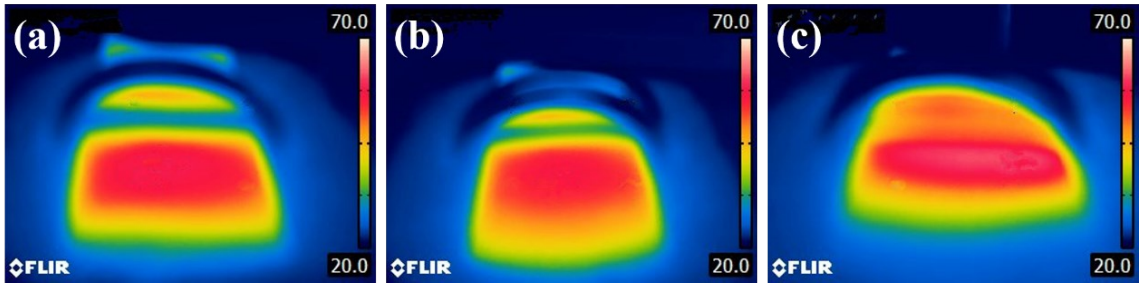

Figure S12. The thermal imaging of the surface of the carbon cloth under different configuration: compact (a, 3 HFCs-a), staircase (b, 3 HFCs-b) and spaced arrangements (c, 3 HFCs-c). The downward sheltered region showed a lower temperature than the surroundings.

We analyzed the solar evaporation efficiency based on the compact array of 5 HFCs using PS foam as the support. As shown in **Figure S13 (a)**, after subtracting this evaporation rate under dark conditions (0.74 kg m^{-2} h^{-1}) from the total evaporation rate under 1 sun illumination (2.10 kg m^{-2} h^{-1}), the evaporation rate is 1.36 kg m^{-2} h^{-1}. The temperature changes with time including the material surface and bulk water was also measured using infrared thermal imager and thermocouple respectively as shown in **Figure S13 (b-c)**. The surface temperature can reach to 30.9 ^{o}C from the initial temperature 21.7 ^{o}C. The evaporation enthalpy and efficiency was calculated as 2465 kJ kg^{-1} and 93%, respectively, which is below the theoretical value in this case (the theoretical value is 1.46 kg m^{-2} h^{-1} when the evaporation enthalpy is 2465 kJ kg^{-1}). Heat losses of this evaporator during solar steam generation, including radiation heat loss (~2.0%), convection heat loss (~3.4%) and conduction heat loss (~3.0%) are calculated. The detailed calculation and energy balance diagram can be seen in Supporting Information (**SII**

and Figure S13). From **Figure S13 (d)**, the conduction heat to bulk water is significantly suppressed due to the absence of water in the hollow pipe (illustrated in **Table S2**), and the convection heat to environment caused by air flowing above hollow fiber membranes is also minimized.

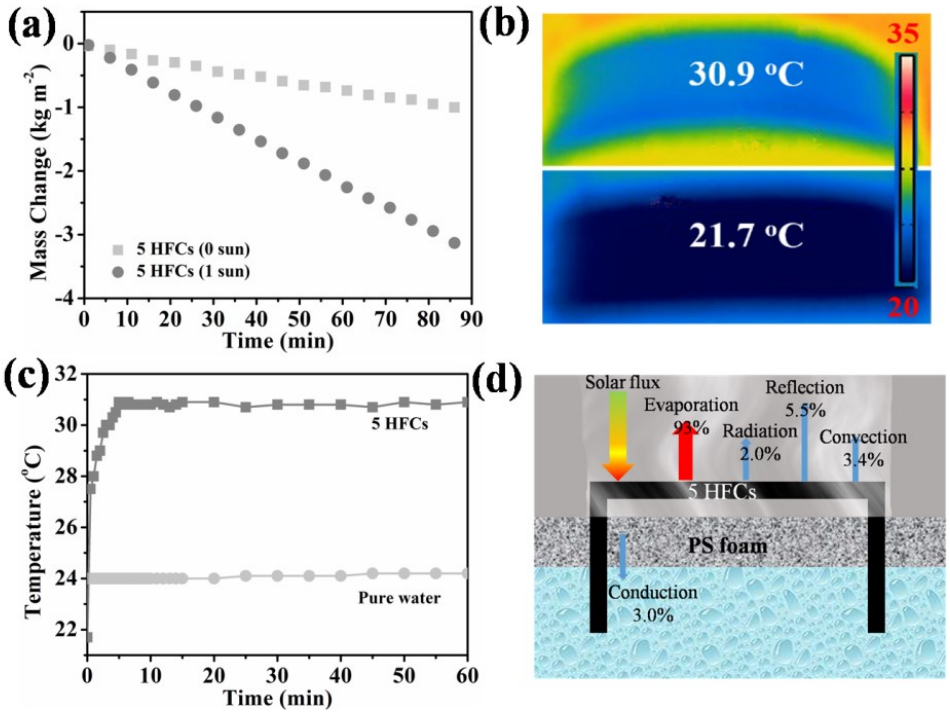

Figure S13. (a) Mass changes with time for 5 HFCs in dark field and 1 sun illumination, (b) Initial and equilibrium temperatures of 5 HFCs, (c) Temperature changes of bulk water and 5 HFCs under 1 sun illumination, (d) Thermal equilibrium for 5 HFCs-compact-PS foam.

As depicted in **Supporting Scheme 1,** the combination of overhead fiber array and base support is apparently an open thermodynamic system, which allows for heat and mass (water and vapor) exchange. The open system is applicable to actual working condition, especially outdoor evaporation under SUN illumination, which can fully exploit the surrounding energy and produce enhanced evaporation. When we discuss about the absorptive base, we consider the temperate field on the base is uniform in staircase and spaced fiber arrangement despite the shielding of the suspended fibers with thin diameter (2.1 mm). We also consider the compact arrayed fibers sheltered the light illumination completely.

Truly isolated physical systems do not exist in reality. In terms of the thermodynamics behavior of the suspended hollow fibers, apart from the direct sun illumination and the below base heat, the boundary of the base has the possibility to provide diffuse reflection, irradiation and convection. However, it is impossible to measure the boundary energy contribution for an

open system. Therefore, we only consider the direct sun illumination and the below base heat as the total energy input source for the calculation of evaporation efficiency.

To better understand the evaporation efficiency and contribution of the extra surrounding energy, apparent efficiency $\boldsymbol{\eta}$, real efficiency $\boldsymbol{\eta_1}$, ideal solar efficiency $\boldsymbol{\eta_2}$ were developed, respectively.

Specifically, we calculated the apparent efficiency $\boldsymbol{\eta}$ based on the direct solar input, which is the same as previous reports. $\boldsymbol{\eta_1}$ was obtained in consideration of the total input of both solar energy and thermal energy from the base. We used $\boldsymbol{\eta_2}$ to calculate the sole evaporation efficiency caused by direct sun illumination while excluding the influence of surrounding energy. Ideally, $\boldsymbol{\eta_2}$ is equal to the light absorption of PTFE/CNT composite in case that the fiber temperature is lower than the base temperature, and there will be no thermal loss occurred. The detailed calculation of the heteromorphic arch-like evaporator under different conditions can be expressed using Equation (S4, S5). The results are listed in **Table S3**.

$$\eta_1 = m' \times (Lv + Q) / (P_{in} + Q_{Extra}) \qquad \text{(S4)}$$

$$\eta_2 = m_1 \times (Lv + Q) / P_{in} \qquad \text{(S5)}$$

where $\boldsymbol{\eta_1}$ and $\boldsymbol{\eta_2}$ represent the real efficiency and ideal solar efficiency respectively. m' is the evaporation rate after subtracting the evaporation rate under dark conditions. m_1 is the evaporation rate directly inspired by the sun illumination. Lv is the latent heat of vaporization of water (Lv (T) = $1.91846\times10^6[T/(T–33.91)]^2$ J/kg, where T is the temperature of vaporization),[26] Q is the sensible heat of water of unit mass ($Q = c(T – T_1)$ J/kg, where c is the specific heat of water, which can be assumed as a constant (4.2 J/g • K), T_1 is the initial temperature of water and P_{in} is the incident solar power (1000 W) on the fiber surface.

It can be seen from **Table S3** that the evaporation rate and efficiency in most cases exceeds the theoretical value under one sun illumination (the theoretical evaporation rate calculated from the evaporation enthalpy 2260 kJ kg^{-1} at 100 ^oC is 1.59 kg m^{-2} h^{-1}). This indicated that extra thermal energy from the base materials including radiation and convection energy, additionally contributed to steam generation.

Table S3. Summary of evaporation efficiency of membrane array with different configuration under 1 sun illumination.

Number	Configuration	Absorptive Base	Evaporation rate (kg m^{-2} h^{-1})			η (%)	η_1 (%)	η_2 (%)
			Total	Natural	Net			
1	/	PS foam	3.73	1.07	2.66	181.7	107.5	94.5
1	/	PVDF membrane	3.63	1.07	2.56	174.6	114.4	94.5
1	/	Carbon cloth	4.88	1.07	3.81	261.3	93.6	94.5
3	Compact	PS foam	2.06	0.70	1.36	93.1	93.1	/
3	Staircase	PS foam	2.60	0.83	1.77	120.9	108.9	94.5
3	Spaced	PS foam	3.14	0.88	2.26	154.7	110.2	94.5
3	Compact	PVDF membrane	2.21	0.72	1.49	102.0	102.0	/
3	Staircase	PVDF membrane	2.43	0.81	1.62	110.7	103.2	94.5
3	Spaced	PVDF membrane	3.01	0.85	2.16	147.9	104.0	94.5
3	Compact	Carbon cloth	2.26	0.71	1.55	106.1	106.1	/
3	Staircase	Carbon cloth	2.91	0.82	2.09	142.5	80.2	94.5
3	Spaced	Carbon cloth	3.35	0.87	2.48	169.1	71.8	94.5
5	Compact	PS foam	2.10	0.74	1.36	93.1	93.1	/
15	Compact	PS foam	1.75	0.47	1.28	87.6	87.6	/
15	Staircase	PS foam	1.88	0.59	1.29	88.3	87.2	/
15	Compact	Carbon cloth	1.80	0.45	1.35	92.4	92.4	/
15	Staircase	Carbon cloth	2.15	0.60	1.55	105.9	76.2	94.5

Detailed efficiency calculations are discussed as follows:

1) Compact arrangement

It is assumed that when multiple fibers are arranged in a compact manner, the base was sheltered and failed to supply heat to the above fiber array. Therefore, the sun illumination was the only energy input without considering the influences of base, where the values of η and η_1 are the same (93.1%, 3-compact-PS foam, 5-compact-PS foam). In practice, the efficiency for 3 HFCs is over 100% when PVDF membrane (102.0%) and carbon cloth (106.1%) are used as base materials, which indicated the boundary diffuse reflection and heat may enhance the real steam generation as the aperture area (A_4) is larger than the illuminated area (A_3). When the

array fiber number was further increased (15 HFCs), the evaporation efficiency decreased accordingly (87.6% for PS foam, 92.4% for carbon cloth) because the boundary area (A_4- A_3) of the base was further narrowed. Ideally, the solar efficiency η_2 is 94.5% for the single fiber and fiber array in staircase or spaced configuration, where there will be no thermal loss through radiation and convection since the fiber temperature is lower than that of the base. For fiber array in compact configuration, it is difficult to calculate the solar efficiency η_2, since heat loss occurred and the boundary energy also influenced the diffuse reflection and thermal supply.

2) Staircase arrangement

As shown in **Figure 5** and **Figure S12**, when the fibers are arranged in a staircase manner, the base surface temperature is higher than that of compact arranged fibers, which therefore generates a higher apparent efficiency η in all cases, e.g. 88.3% for 15-staircase-PS foam and 105.9% for 15-staircase-carbon cloth. The thermal supply from the base influences the apparent efficiency η significantly, 142.5%, 120.9% and 110.7% were obtained, respectively, for 3-staircase fiber array when carbon cloth, PVDF membrane and PS foam was used as the base materials. The real efficiency η_1 was lower than η because we considered the total energy input of solar and base heat for calculation. For example, the real efficiency η_1 of 15-staircase-carbon cloth was 76.2% compared to η (105.9%). However, the staircase configuration was applicable to outdoor evaporation, where the moving sunlight can shine on the base through the staircase fibers from different angle, the phototropistic cylindrical fiber is able to cope with the moving sunlight. Moreover, occupied area can also be saved comparing to spaced manner. Under the same solar intensity and arrangement, the base surface temperature under outdoor illumination is higher than indoor illumination due to the scattering of real sunlight. We chose the outdoor and indoor light intensity of 750 W and found that the surface temperature of the carbon cloth (42 ^{o}C) under outdoor illumination is higher than indoor case (31 ^{o}C) after 20 minutes irradiation.

3) Spaced arrangement

Compared with compact and staircase arrangement, spaced arrangement has the least light shielding effect on base material. Therefore, the corresponding evaporation rate is higher than compact and staircase arrangement. Similar to the single fiber evaporation, the spaced 3-fiber array exhibited higher evaporation rate and apparent efficiency η, e.g. 169.1%, 154.7% and 147.9% when carbon cloth, PS foam and PVDF membrane were used as the base materials, respectively. The real efficiency η_1 values were 71.8%, 110.2% and 104.0%, respectively for 3-spaced-carbon cloth, 3-spaced-PS foam and 3-spaced-PVDF membrane. In case of 3-spaced-carbon cloth, the spaced fibers allow for more sunlight incoming than the case of staircase array.

Higher temperature and more energy were produced to heat the array, and also there will be more heat loss for 3-spaced-carbon cloth. Therefore, we obtained a higher evaporation rate (2.48 kg m^{-2} h^{-1}), higher apparent efficiency (169.1%), but a lower real efficiency (71.8%).

Table S4. Comparison of evaporation rate of various materials under 1 sun illumination.

Materials	Extra energy	Evaporation rate (kg m^{-2} h^{-1})	Ref.
Graphene Oxide	No	1.45	1
PPy coated stainless steel mesh	No	0.92	2
Ti_2O_3 Nanoparticles	No	1.32	26
Carbonized Mushrooms	No	1.475	31
Multifunctional Porous Graphene	No	1.50	36
Black TiO_x Nanoparticles	No	0.80	37
Graphene Sheets Membrane	No	1.62	38
Hierarchical Graphene Foam	No	1.4	39
Paper-Based Reduced Graphene Oxide	No	1.778	40
Porous Hydrophilic Modified NiO	No	1.13	41
Durable Monolithic Polymer	No	1.1687	42
3D Cross-Linked Honeycomb Graphene Foam	No	1.30	43
Monolithic Carbon Sponges	No	1.39	44
Single-Walled Nanotube-MoS_2 Hybrid Film	No	1.0	45
Graphite-Coated Wood.	No	1.15	46
Quasi-Metallic $WO_{2.9}$ Nanorods	No	1.28	47
RGO–MWCNT Photothermal Layer	No	1.22	48
Defect-Abundant Graphene Sheets	No	1.78	49
Black Silver Nanostructures	No	1.38	50
Graphene Oxide-Based Aerogels	No	1.622	51
GO/CNT Layer	No	1.25	52
Selenium-Coated Tellurium Nanomaterials	No	1.323	53
Hierarchically Nanostructured Gels	No	3.2	9
Cellulose with Carbon Black Nanoparticles	Yes	1.62	11
Carbon-Coated Paper	Yes	2.2	12
3D Cylindrical Cup-shaped Structure	Yes	2.04	13
1 HFC/PVDF 1 HFC/PS 1 HFC/Carbon cloth 3 HFCs/Carbon cloth/Spaced 15 HFCs/Carbon cloth/Staircase	Yes	3.63 3.73 4.88 3.35 2.15	This work

Table S5. Weather conditions during outdoor operation in the year of 2019.

Date	Weather	Temperature (°C)
Sept. 15	Sunny	29/23
Sept. 16	Sunny	29/23
Sept. 17	Sunny	28/23
Sept. 18	Sunny	29/22
Sept. 19	Sunny	26/22
Sept. 20	Cloudy	26/20
Sept. 21~22	Typhoon	
Sept. 23	Sunny	26/17
Sept. 24	Sunny	26/14
Sept. 25	Cloudy	27/15
Sept. 26	Sunny	26/16
Sept. 27	Cloudy	26/17
Sept. 28	Sunny	26/19
Sept. 29	Sunny	26/19
Sept. 30	Sunny	26/23
Oct. 1~2	Typhoon	
Oct. 3	Sunny	27/21
Oct. 4	Sunny	29/21

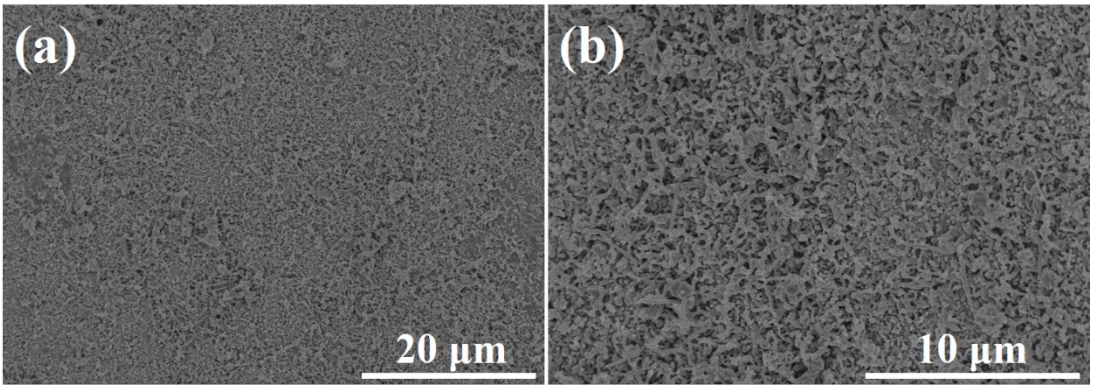

Figure S14. The structure and morphology of HFC after long-term durability test (15 days).

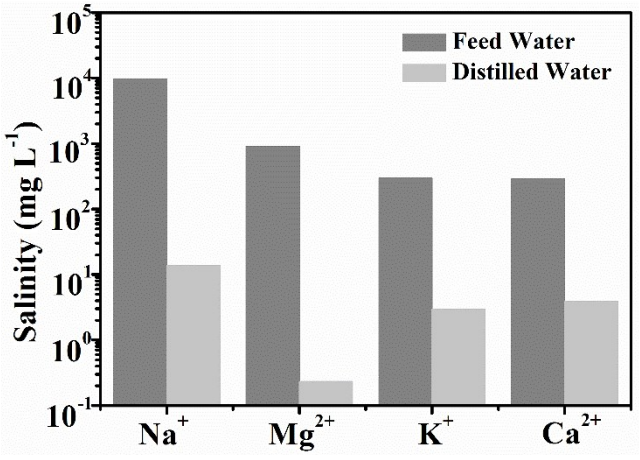

Figure S15. The concentration of four primary ions in simulate seawater before and after solar thermal purification.

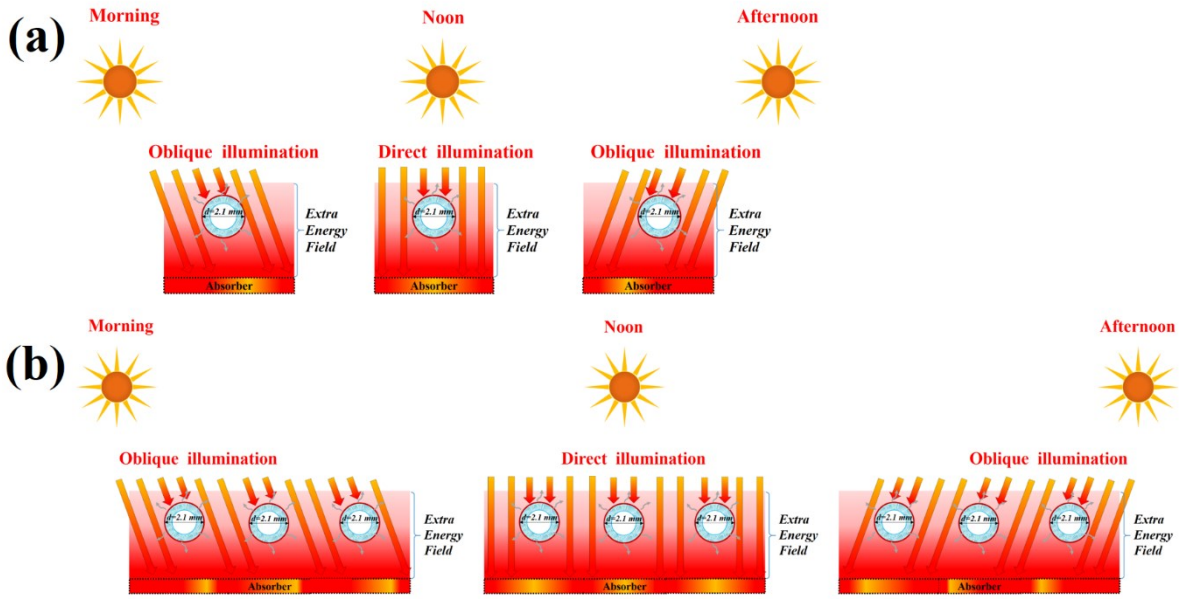

Figure S16. Schematic of high temperature field-assisted steam generation under different time illumination for (a) single fiber and (b) multiple fibers arranged in a spaced manner.

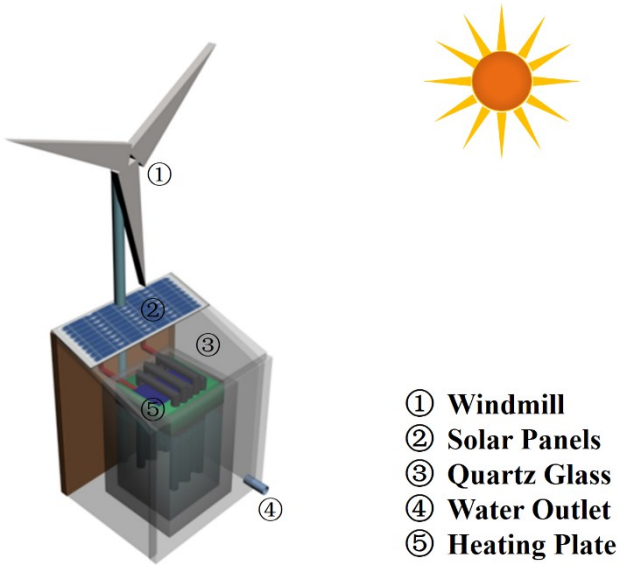

Figure S17. The integration of natural energy e.g. solar irradiation, photothermal power and wind power with PTFE hollow fiber array for enhanced interfacial evaporation.

SI: Mechanism of the energy enhanced solar-to-steam generation for HFC.

The ambient temperature created by the support around single fiber is considered to be the temperature on the surface of the support due to the small diameter of the fiber (~2.1 mm). Therefore, the radiation, convection and conduction heat losses to environment can be ignored

in this case due to ambient temperature is higher than the surface temperature of hollow fiber membrane (**Figure 3d-i**). In this case, the heat transfer process of solar-to-steam generation includes two energy flows: direct solar energy and base heat. The energy transfer process of single fiber used as evaporator can be expressed as the following equations:

$$m'(Lv+Q)=Q_s+Q_e \qquad \text{(S6)}$$

$$Q_s=P_{in}A_1 \qquad \text{(S7)}$$

$$Q_e=-\varepsilon A_2\sigma(T_f^4-T_e^4)-A_2h(T_f-T_e) \qquad \text{(S8)}$$

where, *m'* is the evaporation rate for single fiber used as evaporator after subtracting the evaporation rate under dark conditions, *Lv* is the latent heat of vaporization of water (*Lv* (T)=1.91846×10^6[T/(T–33.91)]^2 J/kg, where T is the temperature of vaporization), Q is the sensible heat of water of unit mass (Q=c(T_2 – T_1) J/Kg, where c is the specific heat of water, which can be assumed as a constant (4.2 J/g K), T_2 is the temperature of vaporization and T_1 is the initial temperature of the water), Q_s is the solar energy, Q_e is the total energy contributed by the support material to the evaporation in the form of heat radiation and heat convection, P_{in} is the solar density and A_1 is the projection area of single fiber, T_f and T_e are the temperatures of fiber surface and support surface, respectively, A_2 is the surface area of single fiber, ε is emissivity, σ is Stefan-Boltzmann constant, h is convective heat transfer coefficient. The calculated results are listed in **Table 1**.

SII: The analysis of heat loss for 5 HFCs.

(1) Radiation:

The radiation heat loss was calculated according to Stefan-Boltzmann equation:

$$\Phi=\varepsilon A_2\sigma\left(T_1^4-T_2^4\right) \qquad \text{(S9)}$$

where Φ (W m^{-2}) is the radiation heat flux, A_2 (m^2) is the surface area which was directly illuminated by sunlight, σ is the Stefan-Boltzmann constant (5.67×10^{-8} W m^{-2} K^{-4}), ε is the emissivity of material supposed as the maximum emissivity of 1 in this paper, T_1 (304.05 K) is the surface temperature of 5 HFPDs at steady state under 1 sun illumination, and T_2 (302.05 K) is the ambient temperature upward the material under 1 sun illumination. Therefore, according to equation (4), the radiation heat flux is ~20 W m^{-2}, which is ~2.0% of the solar flux (1 sun = 1000 W m^{-2}).

(2) Convection:

The convection heat flux was calculated by Newton' law of cooling:

$$Q = hA_2\Delta T \qquad \text{(S10)}$$

where Q (W m^{-2}) is the convection heat flux, h (10 W m^{-2} K^{-1}) is the convection heat transfer coefficient, A_2 (m^2) is the surface area which was directly illuminated by sunlight and ΔT is the different value between the surface temperature and the ambient temperature upward the material under 1 sun illumination (ΔT=2 K). According to equation (5), the convection heat flux is ~34 W m^{-2}, which is ~3.4% of solar energy.

(3) Conduction:

The conduction heat flux was calculated according to the flowing equation:

$$Q = Cm\Delta T \qquad \text{(S11)}$$

where Q is heat loss, C is the specific heat capacity of water (4.2 J $^oC^{-1}$ g^{-1}), m (80 g) is the weight of water used in the experiment, and ΔT (0.2 ^{o}C) is the temperature difference of pure water after and before solar illumination under 1 sun after 1 h. According mentioned above, the conduction heat loss was calculated ~30 W m^{-2}, which is ~3% of solar flux.